Journal of Applied Physics ARTICLE pubs.aip.org/aip/jap

Evidence of non-isentropic release from high residual temperatures in shocked metals measured with ultrafast x-ray diffraction

Cite as: J. Appl. Phys. **136**, 055901 (2024); doi: 10.1063/5.0217779
Submitted: 7 May 2024 · Accepted: 4 July 2024 ·
Published Online: 6 August 2024

View Online Export Citation CrossMark

Hong Yang,[1,a),b)] Michael R. Armstrong,[2,a)] Ryan A. Austin,[2] Harry B. Radousky,[2,a)] Akshat Hetal Patel,[3] Tiwei Wei,[3] Alexander F. Goncharov,[4] Wendy L. Mao,[1,5] Eduardo Granados,[5] Hae Ja Lee,[5] Inhyuk Nam,[5] Bob Nagler,[5] Peter Walter,[5] Jonathan L. Belof,[2] Shaughnessy B. Brown,[5] Vitali Prakapenka,[6] Sergey S. Lobanov,[7] Clemens Prescher,[8] Nicolas Holtgrewe,[4] Elissaios Stavrou,[2] Paulius V. Grivickas,[2] and Arianna E. Gleason[1,5,a)]

AFFILIATIONS

[1]Department of Earth and Planetary Sciences, Stanford University, Stanford, California 94305, USA
[2]Lawrence Livermore National Laboratory, Livermore, California 94550, USA
[3]School of Mechanical Engineering, Purdue University, West Lafayette, Indiana 47907, USA
[4]Earth and Planets Laboratory, Carnegie Institution for Science, Washington, DC 20015, USA
[5]SLAC National Accelerator Laboratory, Menlo Park, California 94025, USA
[6]Center for Advanced Radiation Sources, University of Chicago, Chicago, Illinois 60637, USA
[7]GFZ German Research Center for Geosciences, Telegrafenberg, 14473 Potsdam, Germany
[8]Institute of Earth and Environmental Sciences, University of Freiburg, Freiburg, Germany

[a)]**Authors to whom correspondence should be addressed:** hyang777@stanford.edu; armstrong30@llnl.gov; radousky1@llnl.gov; and ariannag@stanford.edu
[b)]**Present address:** Center for Materials of the Universe, School of Molecular Sciences, Arizona State University, Tempe, AZ 85287, USA

08 August 2025 08:15:29

ABSTRACT

Shock experiments are widely used to understand the mechanical and electronic properties of matter under extreme conditions. However, after shock loading to a Hugoniot state, a clear description of the post-shock thermal state and its impacts on materials is still lacking. We used diffraction patterns from 100-fs x-ray pulses to investigate the temperature evolution of laser-shocked Al–Zr metal film composites at time delays ranging from 5 to 75 ns driven by a 120-ps short-pulse laser. We found significant heating of both Al and Zr after shock release, which can be attributed to heat generated by inelastic deformation. A conventional hydrodynamic model that employs (i) typical descriptions of Al and Zr mechanical strength and (ii) elevated strength responses (which might be attributed to an unknown strain rate dependence) did not fully account for the measured temperature increase, which suggests that other strength-related mechanisms (such as fine-scale void growth) could play an important role in thermal responses under shock wave loading/unloading cycles. Our results suggest that a significant portion of the total shock energy delivered by lasers becomes heat due to defect-facilitated plastic work, leaving less converted to kinetic energy. This heating effect may be common in laser-shocked experiments but has not been well acknowledged. High post-shock temperatures may induce phase transformation of materials during shock release. Another implication for the study is the preservability of magnetic records from planetary surfaces that have a shock history from frequent impact events.

© 2024 Author(s). All article content, except where otherwise noted, is licensed under a Creative Commons Attribution-NonCommercial 4.0 International (CC BY-NC) license (https://creativecommons.org/licenses/by-nc/4.0/). https://doi.org/10.1063/5.0217779

I. INTRODUCTION

A shock wave is a large-amplitude mechanical wave across which pressure, density, particle velocity, temperature, and other material properties change nearly discontinuously.[1] The shock compression process is thermodynamically irreversible, where a substantial portion of energy in a shock wave goes into raising the entropy and temperature of the material. While the pressure, volume, and energy across the shock front are determined by the Rankine–Hugoniot equations, the temperature depends on the distribution of this energy across various possibilities such as lattice vibrations, bond dissociation, and plastic work. Moreover, calculating the residual temperatures once the shock is released involves further challenges. This suggests the need to measure the temperature experimentally, but determining temperatures with micrometer-level spatial resolution and nanosecond temporal resolution needed for laser-shocked samples is challenging.

Several methods have been developed to determine the temperature of samples under dynamic compression conditions. For materials shocked to very high temperatures ($\gtrsim$0.3 eV, 3500 K or higher), optical pyrometry is often considered the gold standard by assuming that the heated sample is a gray-body emitter.[2] Streaked optical pyrometry (SOP) can be used to infer the time variation in temperature[3–6] but is only sensitive to the sample surface for opaque materials. Time-resolved Raman spectroscopy offers another method to track temperature. By examining the height difference between the Stokes and anti-Stokes lines, temperatures up to several thousand Kelvin can be derived.[7] Using the temperature dependence of the Debye–Waller factor, which can be deduced from EXAFS spectra, one can also determine the temperature of shocked materials, assuming that thermal contributions dominate Debye–Waller factor variation under shock conditions.[8,9] Still, other approaches have been explored, including embedded thermal gauge layers, where thermal histories are extracted from resistance changes in thin metal layers (e.g., thermistors[10]), or optical sensors;[11] however, these methods often cannot be applied to short time scale experiments. In many cases, it remains challenging to deconvolve compressional vs thermal contributions, especially at shorter timescales, i.e., before shock rarefaction and release waves have traversed the sample multiple times. The integration time for these methods to build significant signal-to-noise ratios can be long, which hinders their application to experiments with high temporal resolution demands.

In this paper, we used ultra-fast x-ray probes to track the thermal response of aluminum (Al) and zirconium (Zr) on shock release from experiments outlined in our previous studies.[12,13] We quantified a thermal effect lasting to long timescales (tens of nanoseconds after cessation of picosecond shock compression), termed residual temperatures, with unprecedented spatial and temporal resolutions using the lattice expansion determined by *in situ* x-ray diffraction (XRD). Measurements from ultrafast XRD measurements were collected at different time delays to obtain the time history of residual temperature increases. We further used thermal conduction simulations to understand this time evolution of temperatures and found a high temperature of Zr right after shock release. Our results indicate that plastic work induced heating, lasting over tens of nanoseconds and indicating a non-isentropic release pathway. We believe this significant heating could exist in many laser-shock experiments. As the temperature influences almost every material property, this can certainly provide an alternative interpretation of experimental results of shock release.

II. METHODS

A. Temperature determined from x-ray diffraction

Fast compression experiments were conducted at the matter in extreme conditions (MEC) station of the LINAC Coherent Light Source (LCLS) at SLAC.[12,13] The x-ray diffraction patterns collected in only 100 fs were enabled by a high-flux x-ray free electron laser (XFEL) at SLAC. We prepared the Zr/Al targets using a sputter coating method and checked the composition with x-ray photoelectron spectroscopy (XPS). Details of the preparation and characterization of the Zr/Al metal composites can be found in previous reports.[12,13] The Zr/Al metal film layers were compressed by a 120-ps duration drive laser with total energies of 2.5, 25, and 30 mJ, as shown in Fig. 1. Peak pressures in the Zr/Al layers were estimated to be 13/10, 33/27, and 46/36 GPa, respectively (Table I).[13] Lattice constants of Al and Zr were examined by 100 fs duration x-ray diffraction at different time delays ranging from 1 to 75 ns. It is worth noting that Al has a sufficiently large thermal expansion coefficient (2.3×10^{-5} K^{-1})[14] for tracking the temperature change by lattice expansion. On the other hand, the relatively low thermal expansion coefficient (5.8×10^{-6} K^{-1})[15] of Zr and its broad peak shape (FWHM = 0.6°–0.7°) (Fig. 2) only allows for temperature determination with a resolution of ~800–1000 K, and we, therefore, do not include the Zr temperature results from XRD in this study.

To collect the XRD data, charge-integrating detectors, specifically Cornell-SLAC Pixel Array Detectors (CSPADs), were used at a fixed distance and calibrated with CeO_2 and Al powder standards. Integration of two-dimensional XRD patterns and background subtraction were processed in Dioptas version 0.5.2[16] as shown in Fig. 2. Al ⟨111⟩ and ⟨200⟩ peak positions as a function of lattice constant a were fitted in Mathematica using a Lorentz function.

B. Heat conduction simulations

To understand the temperature change in Al and infer the Zr temperatures from 5 to 80 ns (Fig. 3), we conducted a heat conduction simulation within the ANSYS workbench. The transient heat conduction equation is solved across the composite domain through the finite element method (FEM). Temperature-dependent thermal properties of Al[14,17] and Zr[18] are used to accurately capture the heat transfer. At such high temperatures, the thermal properties are strongly dependent on temperature. The initial temperature for aluminum was set to the experimental value for the corresponding drive energy, whereas the initial temperature for zirconium is estimated from these simulations based on the aluminum data. A range of initial temperatures is systematically evaluated, and the resulting aluminum temperature is compared with the experimental data to determine an appropriate initial zirconium temperature. For the 2.5, 25, and 35 mJ cases, the range of the initial Zr temperature values is 1000–1500, 1500–1900, and 1550–1950 K, respectively (Fig. 4). The upper limit of the derived range is based on the maximum initial temperature of Zr, which does not lead to the melting of Al in simulations, as melting was not observed in the x-ray diffraction data.

08 August 2025 08:15:29

© Author(s) 2024

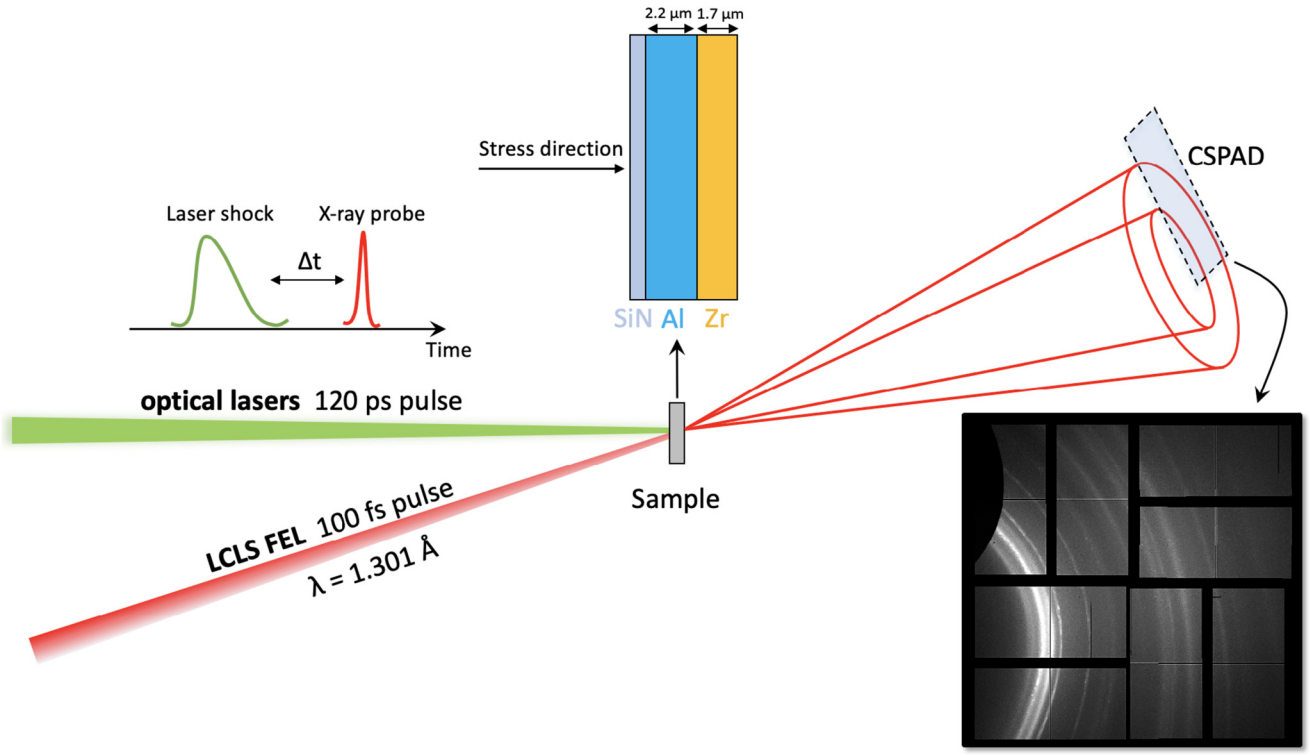


FIG. 1. Schematic of the experimental setup of the short-pulse laser shock experiments. Data were collected at the MEC end-station of LCLS with the sample and drive conditions described elsewhere.[12,13]

08 August 2025 08:15:29

Additionally, it is assumed that the temperature rises due to the laser being confined to a radius of 35 μm,[13] while the remaining portion of the composite remains at room temperature. Figure 4 illustrates the variation in average Al and Zr temperatures with time for different drive energies. As expected, the temperature of Al begins to rise as heat diffuses from Zr to Al.

To check whether thermal radiation significantly cooled the sample, we simulate Zr/Al temperature evolution at the later stage with heat conduction only. We found that including radiation cooling does not change the temperature profiles, and our assumptions of ignoring heat radiation are valid.

C. Hydrodynamic simulations

To further understand the deformation and heating of Zr and Al during shock wave loading and release, we performed continuum hydrodynamic simulations of the initial stage of the experiment (up to a time of ~1 ns) followed by continuum thermal diffusion simulations after release (>3 ns after the drive). The continuum thermal diffusion modeling aimed to track the thermal conduction between the Al and Zr layers after the shock wave loading/unloading cycle and capture initial thermal conditions that are responsible for the longer time scale temperature response out to 80 ns.

To obtain the estimates of temperature and dissipated energy, we employed 1D simulations of shock wave loading in the hydrodynamics code ALE3D.[19] The pressure boundary condition was generated using an empirical calibration from existing data[12,20] and designed to emulate the laser drive. A Mie–Gruneisen equation of state was used for the pressure–volume responses of the Al and Zr layers. The simulations are locally adiabatic, with temperatures obtained from the differences between internal energy and unshocked room-temperature energy and a constant heat capacity (Fig. 5). Here, the equation of state (EOS) does not describe any phase transformations of Zr or Al (e.g., melting). To estimate the heating from plastic work, the model employs a Steinberg–Guinan model of strength, using published parameterizations for Al and Zr.[21,22] In the model, dissipative work occurs at each loading and unloading step, with contributions from both deviatoric plastic stress–strain work and numerical (volume) viscosity. This model does not include any heating from fine scale mechanisms associated with spallation (e.g., void nucleation and growth and/or shear localization). In addition to models with realistic strength values, we also performed simulations with elevated strength (with strength values doubled) and obtained only a modest increase (<12%) in post-shock temperatures [Fig. 5(b)].

III. RESULTS AND DISCUSSION

A. XRD results

Interestingly, for the XRD patterns of Al under shock loading, even at late time delays after shock compression and release had

© Author(s) 2024

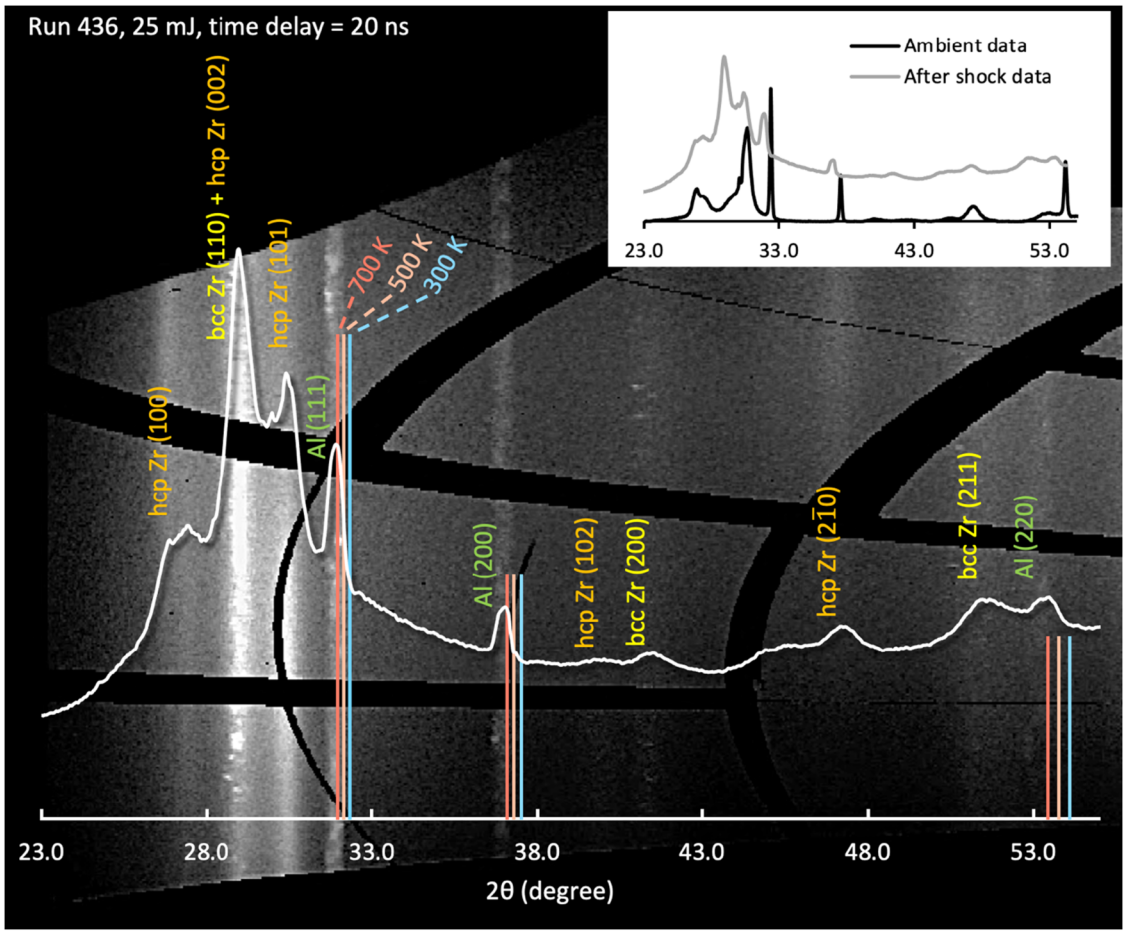


FIG. 2. Caked two-dimensional XRD pattern and the corresponding integrated pattern. Intensities are shown as a function of the scattering angle for a 25 mJ drive energy probed at a 20 ns time delay. Vertical lines indicate expected peak positions for Al at different temperatures, based on Lu *et al.*, 2005,[14] labeled in the figure with a color code. Blue lines are Al at ambient temperature. Line height corresponds to the expected peak intensities. A clear lattice expansion of Al can be identified from the peak positions. bcc-Structured Zr transformed from hcp-Zr can be identified with a new set of diffraction peaks. The inset shows pre-shot (i.e., ambient conditions) and *in situ* shocked diffraction patterns.

08 August 2025 08:15:29

been completed, the peak position of each metal indicated a systematic increase in *d*-spacing. Several precautions were considered before we attributed this effect to thermal strain, including shot-to-shot self-amplified spontaneous emission (SASE), XFEL pulse wavelength fluctuation, and detector-to-sample distance reduction due to shocked sample motion toward the detector. The x-ray wavelength fluctuation was insignificant. To calculate the sample-detector distance change, Zr Hugoniot data[23] were used to estimate the maximum surface velocity and the distance the sample could have traveled at XRD probe times. The resulting distance was less than 0.2 mm, such that the adjusted detector-to-sample has a negligible effect on the measured peak d-spacings and derived lattice constants. Using traditional radiation hydrodynamics codes,[19] shock stresses induced by the drive laser are completely released by a few ns for all three energies. Therefore, we conclude that the Al peak position shifts are entirely due to thermal expansion. Using peak position information, we calculated the temperature of Al using a thermal EOS[14] as shown in Figs. 2 and 3.

Uncertainties in the Al lattice constant were estimated by combining both the SASE XFEL wavelength jitter and the peak fitting statistical errors using 40 independent x-ray measurements of pre-shock face-centered cubic (fcc)-Al patterns, resulting in a standard derivation of 0.003 Å. The Al peak fitting statistical errors were typically 0.001–0.002 Å. The total uncertainty of lattice spacing was further propagated to temperature uncertainty shown in Fig. 3, assuming that the uncertainty of the thermal expansion coefficient is negligible.[14]

Body-centered cubic (bcc) structured Zr was observed in 25 and 30 mJ runs at time delays from 1.4 to 75 ns. This bcc-Zr is only stable in the high temperature regime, which indicates that a

© Author(s) 2024

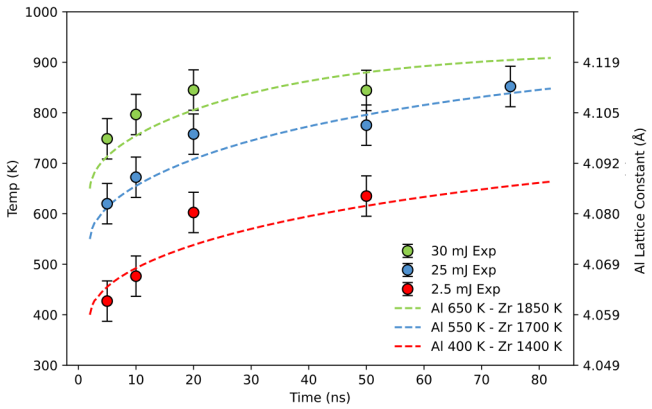


FIG. 3. Temperature history of the Al layer determined from lattice expansion following the laser-driven dynamic compression events. The arrival of the drive laser is t = 0 ns. Dashed lines are theoretical simulations of the temperature evolution of an Al layer, in contact with a Zr layer with higher temperature. The initial temperatures of the Al and Zr layers of heat conduction simulations are provided in the figure caption.

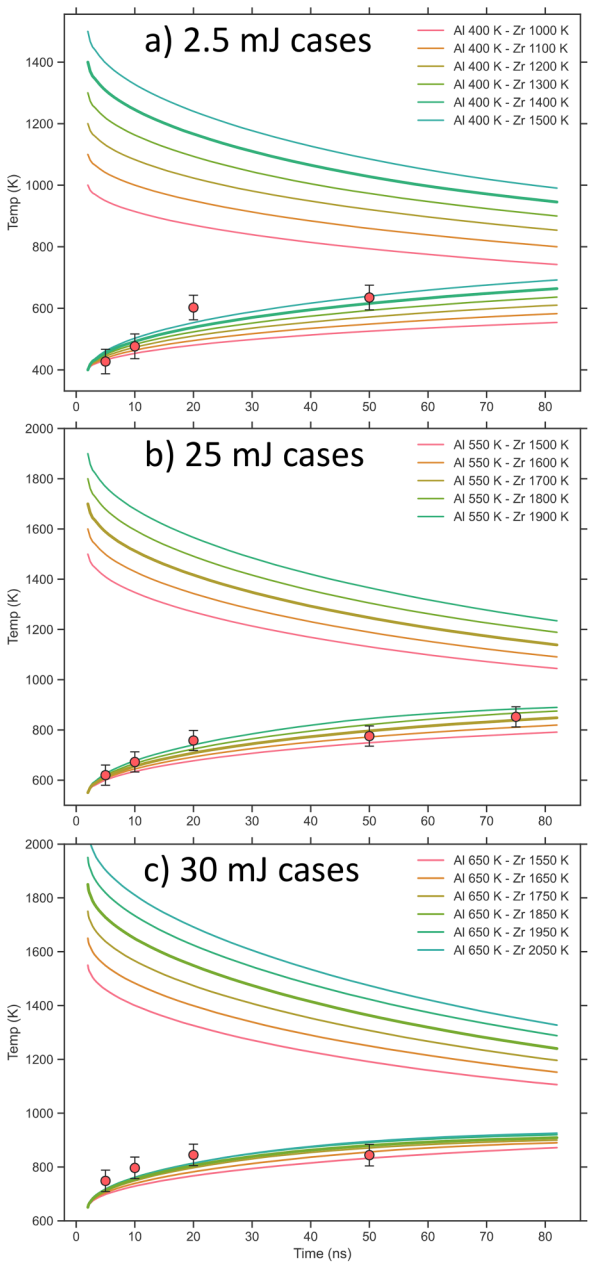


FIG. 4. Continuum heat conduction model results. Variation in average Al and Zr temperatures with time for difference cases: (a) 2.5, (b) 25, and (c) 35 mJ. The initial temperatures of Al and Zr for different conduction models are given in the figure caption. Cases highlighted by thick lines correspond to those shown in Fig. 3. In all simulated cases, no Al melting was found.

part of the Zr sample volume probed is at least at temperatures more than 1150 K.

In thin film multilayers, the strain at the interface of two materials, such as Al and Zr, remains consistent prior to mechanical failure. This phenomenon could potentially influence temperature estimations derived from thermal strain. However, we find that this effect would primarily result in an underestimation of temperature, which does not critically undermine our conclusions.

At the Al–Zr interface, strain is influenced not only by temperature variations but also by the intermetallic bonding between these layers. Given the disparate thermal expansion coefficients of Al and Zr, differential expansion of these layers is anticipated. Nevertheless, the mechanical robustness of Zr is likely to counteract this misalignment. Consequently, while our temperature estimates based on the strain-temperature relationship might be affected by this strength constraint, the significantly higher thermal expansion coefficient of Al implies that this mechanical aspect would primarily suppress excessive displacement. Hence, our temperature assessments, though slightly conservative, remain valid and well beyond the model estimation without a significant plastic heating effect.

The effects of Al deformation on XRD peaks from thermal gradient-induced deviatoric stress are also considered. The strength of pure Al is in the tens MPa range at ambient temperature[24] and drops substantially upon heating to hundreds of degrees Celsius.[25] As such, we do not expect substantial deviatoric stresses from thermal gradients to be supported in aluminum—such stresses will plastically relax for temperature gradients much less than the temperatures we estimate. For the same reason, we do not expect significant temperature-induced stresses at the Zr/Al boundary.

In Fig. 3, we show the inferred temperatures determined via the measurements of thermal expansion at different time delays. We report data after 5 ns to ensure that shock wave reverberations have dissipated, so lattice expansion only occurs due to elevated temperature at ambient pressure. As seen in Fig. 5, we see reverberations which continue to at least beyond 1 nanosecond. Five nanoseconds is 5–10 reverberation times subsequent to shock, which is sufficient for the pressure to release to zero uniformly over the

08 August 2025 08:15:29

© Author(s) 2024

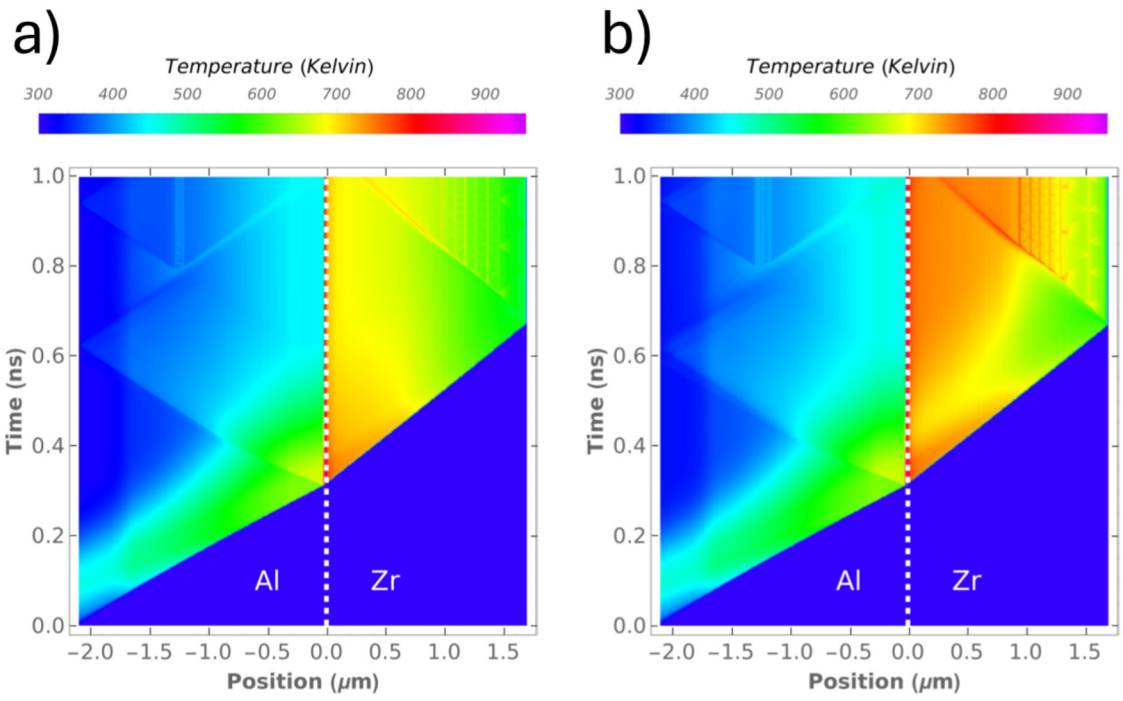


FIG. 5. Temperatures derived from hydrodynamic simulations of the 25 mJ drive for a strength model with (a) conventional parameterizations, and (b) elevated strength values (two times nominal flow resistance). The vertical white dashed lines indicate the Al/Zr interface. The laser is incident from the left, driving a shock wave front through Al, which arrives at the Al/Zr interface around 320 ps.

08 August 2025 08:15:29

entire sample. At early times (<5 ns), we observe fluctuations of the lattice constant that we associate with these reverberations. However, this is not included in Figs. 3 and 4 since we have no deterministic way to separate pressure and temperature contributions to the lattice strain. On the other hand, the averages of short-time scale strains (and correlated temperatures) are still noticeably well beyond the temperature predicted by hydrodynamic simulations (Fig. 6).

B. Heat conduction simulations

Since Zr diffraction peaks are wide and Zr thermal expansion is not as significant as Al per unit of temperature change, we attempted to use Al temperature changes (>5 ns) to determine the range of Zr temperatures using heat conduction models. We modeled the heat conduction between Zr and Al layers, using the later stage of temperature change. Al temperature kept increasing after 20 ns, while Zr temperature dropped by ~200 K, as heat was being transferred from higher temperature Zr to lower temperature Al. We reproduced this observation in a heat conduction model, using the sample design with Al and Zr thermal properties and setting an initial homogeneous temperature of Al and Zr at 700 and 2100 K in the shock heated with a radius of 35 μm, respectively (Fig. 4). This means that the temperature evolution in Al and Zr after pressure release is well described by the thermal conduction process. Note that in reality, we do not expect heat conduction to start from two layers with homogeneous thermal states, and this model only serves as a first-order description of the heat conduction process between metal layers and this was not intended to fit the data perfectly.

C. Hydrodynamic simulations

The significantly elevated temperatures (Table I) at late times (>5 ns) for Al indicate considerable heat coming from the Zr layer, given the sample is thermally isolated in vacuum. This led us to investigate the thermal states for both Al and Zr at early times (<5 ns). For Al, the average temperatures for the 2.5, 25, and 30 mJ cases prior to 5 ns are ~420, 610, and 720, which are noticeably higher than the Al temperatures predicted by hydrodynamic simulations (Fig. 6). We also did not observe a monotonic increase in thermal strain or temperature at 1–5 ns, as predicted from the heat conduction models, possibly due to strain fluctuations associated with wave reverberations. Furthermore, no thermoelastic cooling due to pressure release was visible in Al temperatures at early times from the diffraction data. However, this thermoelastic cooling was predicted to be ~80–130 K for Al by hydrodynamic simulations. The lack of cooling was thought to be an effect of plastic work due to defects.[26] For Zr, the inferred initial temperatures constrained by heat conduction models also exceed the hydrodynamic model results by large amounts (see Fig. 6). From the perspective of energy conservation, besides accelerating the bulk sample to their

© Author(s) 2024

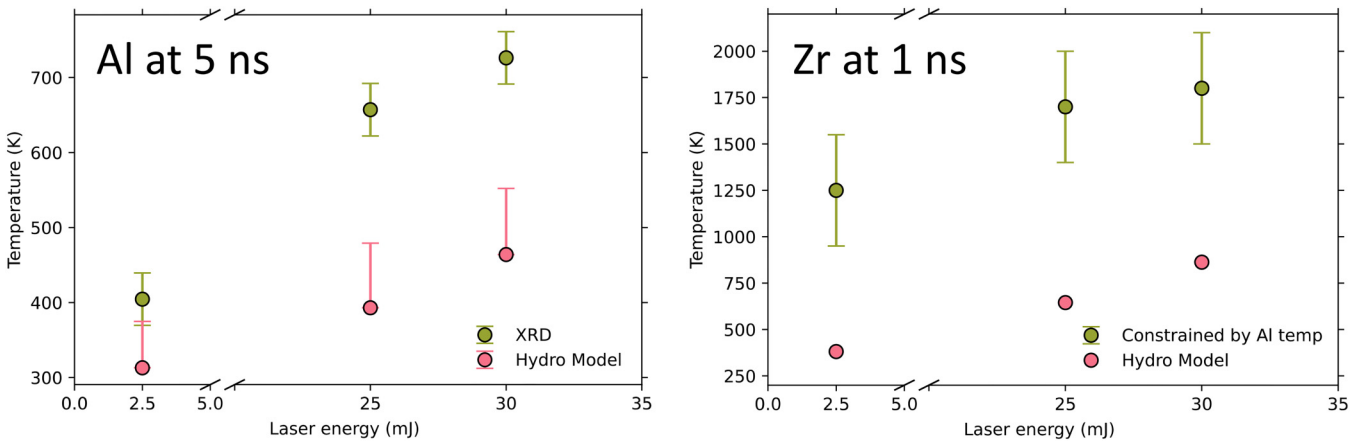


FIG. 6. Comparison of temperatures at early time scales from experimental results and hydrodynamic simulations. For the Al dataset, the XRD results are taken at 5 ns after the start of laser ablation, which produced the shock wave. For the hydrodynamic model, we plotted the data at 1 ns and used upper error bars to represent the temperature increase up to 5 ns due to thermal conduction from Zr. In this case, we used the most conservative estimation based on high Zr temperatures from the heat conduction model at 1 ns. For the Zr dataset, the initial temperatures were obtained from heat conduction (constrained by Al temperature observations) and hydrodynamic models. For both materials, the elevated residual temperatures based on the heat conduction model also showcase the uncaptured portion of thermal energy in the hydrodynamic models.

final particle speed, the shock energy has to be converted to compressing or breaking chemical bonds. The compressing part can be possibly recovered through thermal-elastic cooling while the breaking bond part is irreversible and can possibly explain our observations here. Additionally, a significant portion of heating from plastic work can be attributed to void growth associated with spallation-type behavior.[27,28] In such cases, various defects may serve as nucleation centers, including impurities, second-phase particles, and grain boundaries.

Our target material selection allows the capture of thermal effects in these nanosecond scale experiments. Specifically, Zr has high strength that efficiently converts shock energy into heat, while Al has a high thermal expansion coefficient that makes this heat visible in XRD patterns. We suspect that this plastic-work-induced heating also occurs in several previous studies.[29–31] However, due to the relatively early time scale of x-ray probing or low thermal expansion of the materials used, this effect is yet to be confidently resolved in these experiments. We also believe the higher-than-expected residual temperature is likely a consequence of the small scale of these experiments, and that such effects are absent from millimeter-scale experiments done for the typical Hugoniot datasets. This indicates that plastic heating is likely uneven and primarily associated with the boundary regions.

TABLE I. Peak shock pressures, shock Hugoniot temperatures, and the released temperatures of the samples.

Laser energy (mJ)	Layer	Peak pressure (GPa)	Hugoniot temp[a] (K)	Release temp[b] (K)	Release temp[a] (K)
2.5	Al	10	336	400 ± 40	313
	Zr	13	355	1300 ± 250	381
25	Al	27	483	550 ± 40	393
	Zr	33	610	1700 ± 250	645
30	Al	36	607	650 ± 40	464
	Zr	46	820	1800 ± 250	863

[a]From hydrodynamic simulations.
[b]From XRD and thermal conduction model constraints.

IV. CONCLUSION

In this paper, we have shown that it is feasible to measure residual temperatures following ultrafast shock compression out to late times. In particular, a short-pulse (130 ps) shock was shown to exhibit significant heating after release (out to 80 ns elapsed time), exceeding expectations based on conventional models of rate-independent high-pressure plasticity, which is important for thermodynamic modeling of the effects of shock compression and release. X-ray diffraction has been shown to be an effective thermometer to measure this temperature. We believe that this opens a new avenue of research for looking at shock temperatures since this likely occurs in a wide range of shock compression experiments but is not generally acknowledged or measured. We note that this measurement requires a thin target and availability of x-ray diffraction at times long after shock release. This requires no additional experimental infrastructure, and we propose that many experiments would benefit from following the temperature history for longer times than has normally been acknowledged as relevant.

An area of application where this new residual temperature phenomenon is important is studying the thermal effects of shock release for geo-materials during cratering processes.[32,33] Thermal effects during shock events can be critical for examining the shock-

08 August 2025 08:15:29

© Author(s) 2024

modified paleomagnetic records in lunar basalts. Magnetization of these rocks is used to recover the lunar dynamo behavior at times when rocks were cooled below their Curie/Néel temperature.[34,35] However, if basalt was later shocked and heated above a certain temperature, its magnetic record would be reset and not represent the original paleomagnetic field. Thus, knowing how much heating is accompanied by shock processes at late times, including residual temperatures, is necessary to evaluate these paleomagnetic records in rocks.

SUPPLEMENTARY MATERIAL

See the supplementary material for hydrodynamic simulation results for 2.5 and 30 mJ cases.

ACKNOWLEDGMENTS

H.Y., A.E.G., and W.L.M. acknowledge support by the Geophysics Program at NSF (No. EAR2049620). Lawrence Livermore National Laboratory is operated by Lawrence Livermore National Security, LLC, for the U.S. Department of Energy, National Nuclear Security Administration under Contract No. DE-AC52-07NA27344. This work was partially sponsored by the Department of Defense, Defense Threat Reduction Agency under the Materials Science in Extreme Environments University Research Alliance, No. HDTRA1-20-2-0001. This research was also supported by LLNL Laboratory Directed Research and Development Strategic Initiative 21-SI-006 and Exploratory Research 16-ERD037. The content of the information does not necessarily reflect the position or the policy of the federal government, and no official endorsement should be inferred. Use of the Linac Coherent Light Source (LCLS), SLAC National Accelerator Laboratory, was supported by the U.S. Department of Energy Office of Science, Office of Basic Energy Sciences under Contract No. DE-AC02-76SF00515. The MEC instrument is supported by the U.S. Department of Energy, Office of Science, Office of Fusion Energy Sciences under Contract No. SF00515. We greatly appreciate discussions with Gaia Righi and Hye-sook Park. We also thank the reviewers and editor for their comments, which greatly improved this manuscript.

AUTHOR DECLARATIONS

Conflict of Interest

The authors have no conflicts to disclose.

Author Contributions

Hong Yang: Conceptualization (equal); Data curation (equal); Formal analysis (lead); Methodology (equal); Project administration (equal); Software (equal); Validation (equal); Visualization (lead); Writing – original draft (lead); Writing – review & editing (equal). **Michael R. Armstrong:** Conceptualization (equal); Data curation (equal); Formal analysis (equal); Funding acquisition (equal); Investigation (equal); Methodology (equal); Project administration (equal); Resources (equal); Supervision (equal); Validation (equal); Visualization (equal); Writing – review & editing (equal). **Ryan A. Austin:** Conceptualization (equal); Data curation (equal); Formal analysis (equal); Funding acquisition (equal); Investigation (lead); Methodology (equal); Project administration (equal); Resources (equal); Software (equal); Supervision (equal); Validation (equal); Visualization (equal); Writing – review & editing (equal). **Harry B. Radousky:** Conceptualization (equal); Funding acquisition (equal); Investigation (lead); Methodology (supporting); Project administration (equal); Resources (equal); Supervision (equal); Writing – review & editing (equal). **Akshat Hetal Patel:** Data curation (equal); Formal analysis (equal); Funding acquisition (supporting); Methodology (equal); Software (equal); Validation (equal); Visualization (equal); Writing – review & editing (equal). **Tiwei Wei:** Data curation (equal); Formal analysis (equal); Methodology (equal); Resources (equal); Software (equal); Supervision (equal); Validation (equal); Visualization (equal); Writing – review & editing (equal). **Alexander F. Goncharov:** Investigation (equal); Writing – review & editing (equal). **Wendy L. Mao:** Funding acquisition (supporting); Investigation (equal); Resources (equal); Supervision (equal); Writing – review & editing (equal). **Eduardo Granados:** Investigation (equal); Writing – review & editing (equal). **Hae Ja Lee:** Investigation (equal); Writing – review & editing (equal). **Inhyuk Nam:** Investigation (equal); Writing – review & editing (equal). **Bob Nagler:** Investigation (equal); Software (equal); Writing – review & editing (equal). **Peter Walter:** Investigation (equal); Writing – review & editing (equal). **Jonathan L. Belof:** Investigation (equal); Writing – review & editing (equal). **Shaughnessy B. Brown:** Investigation (equal); Writing – review & editing (equal). **Vitali Prakapenka:** Investigation (equal); Writing – review & editing (equal). **Sergey S. Lobanov:** Investigation (equal); Writing – review & editing (equal). **Clemens Prescher:** Investigation (equal); Software (equal); Writing – review & editing (equal). **Nicolas Holtgrewe:** Investigation (equal); Writing – review & editing (equal). **Elissaios Stavrou:** Investigation (equal); Writing – review & editing (equal). **Paulius V. Grivickas:** Investigation (equal); Writing – review & editing (equal). **Arianna E. Gleason:** Conceptualization (equal); Data curation (equal); Funding acquisition (equal); Investigation (lead); Methodology (equal); Project administration (equal); Resources (equal); Supervision (equal); Writing – review & editing (equal).

08 August 2025 08:15:29

DATA AVAILABILITY

The data that support the findings of this study are available from the corresponding authors upon reasonable request.

REFERENCES

[1]P. D. Asimow, "Dynamic compression," in *Treatise on Geophysics* (Elsevier, 2015), pp. 393–416.
[2]H. B. Radousky and A. C. Mitchell, "A fast UV/visible pyrometer for shock temperature measurements to 20 000 K," Rev. Sci. Instrum. **60**(12), 3707–3710 (1989).
[3]J. E. Miller, T. R. Boehly, A. Melchior, D. D. Meyerhofer, P. M. Celliers, J. H. Eggert, D. G. Hicks, C. M. Sorce, J. A. Oertel, and P. M. Emmel, "Streaked optical pyrometer system for laser-driven shock-wave experiments on OMEGA," Rev. Sci. Instrum. **78**(3), 034903 (2007).
[4]H.-S. Park, S. J. M. Ali, P. M. Celliers, F. Coppari, J. Eggert, A. Krygier, A. E. Lazicki, J. M. Mcnaney, M. Millot, Y. Ping, R. E. Rudd, B. A. Remington, H. Sio, R. F. Smith, M. D. Knudson, and E. E. McBride, "Techniques for studying

© Author(s) 2024

materials under extreme states of high energy density compression," Phys. Plasmas **28**(6), 060901 (2021).
[5]A. Seifter, "Post-Shock temperature measurements of aluminum," in *AIP Conference Proceedings* (AIP, Baltimore, MD, 2006), pp. 139–142.
[6]S. T. Stewart, "Post-Shock temperature and free surface velocity measurements of basalt," in *AIP Conference Proceedings* (AIP, Baltimore, MD, 2006), pp. 1484–1487.
[7]A. Sato, S. Oguchi, and K. G. Nakamura, "Temperature measurement of carbon tetrachloride under laser shock compression by nanosecond Raman spectroscopy," Chem. Phys. Lett. **445**(1–3), 28–31 (2007).
[8]Y. Ping, F. Coppari, D. G. Hicks, B. Yaakobi, D. E. Fratanduono, S. Hamel, J. H. Eggert, J. R. Rygg, R. F. Smith, D. C. Swift, D. G. Braun, T. R. Boehly, and G. W. Collins, "Solid iron compressed up to 560 GPa," Phys. Rev. Lett. **111**(6), 065501 (2013).
[9]H. Sio, A. Krygier, D. G. Braun, R. E. Rudd, S. A. Bonev, F. Coppari, M. Millot, D. E. Fratanduono, N. Bhandarkar, M. Bitter, D. K. Bradley, P. C. Efthimion, J. H. Eggert, L. Gao, K. W. Hill, R. Hood, W. Hsing, N. Izumi, G. Kemp, B. Kozioziemski, O. L. Landen, K. Le Galloudec, T. E. Lockard, A. Mackinnon, J. M. McNaney, N. Ose, H.-S. Park, B. A. Remington, M. B. Schneider, S. Stoupin, D. B. Thorn, S. Vonhof, C. J. Wu, and Y. Ping, "Extended X-ray absorption fine structure of dynamically-compressed copper up to 1 terapascal," Nat. Commun. **14**(1), 7046 (2023).
[10]Z. Rosenberg and Y. Partom, "Direct measurement of temperature in shock-loaded polymethylmethacrylate with very thin copper thermistors," J. Appl. Phys. **56**(7), 1921–1926 (1984).
[11]D. H. Dolan, C. Seagle, and T. Ao, Dynamic temperature measurements with embedded optical sensors (2013), pp. SAND2013-8203, 1096517, 476702.
[12]H. B. Radousky, M. R. Armstrong, R. A. Austin, E. Stavrou, S. Brown, A. A. Chernov, A. E. Gleason, E. Granados, P. Grivickas, N. Holtgrewe, H. J. Lee, S. S. Lobanov, B. Nagler, I. Nam, V. Prakapenka, C. Prescher, P. Walter, A. F. Goncharov, and J. L. Belof, "Melting and refreezing of zirconium observed using ultrafast x-ray diffraction," Phys. Rev. Res. **2**(1), 013192 (2020).
[13]M. R. Armstrong, H. B. Radousky, R. A. Austin, E. Stavrou, H. Zong, G. J. Ackland, S. Brown, J. C. Crowhurst, A. E. Gleason, E. Granados, P. Grivickas, N. Holtgrewe, H. J. Lee, T. T. Li, S. Lobanov, J. T. McKeown, B. Nagler, I. Nam, A. J. Nelson, V. Prakapenka, C. Prescher, J. D. Roehling, N. E. Teslich, P. Walter, A. F. Goncharov, and J. L. Belof, "Observation of fundamental mechanisms in compression-induced phase transformations using ultrafast X-ray diffraction," JOM **73**(7), 2185–2193 (2021).
[14]X. Lu, M. Selleby, and B. Sundman, "Theoretical modeling of molar volume and thermal expansion," Acta Mater. **53**(8), 2259–2272 (2005).
[15]R. B. Russell, "Coefficients of thermal expansion for zirconium," JOM **6**, 1045–1052 (1954).
[16]C. Prescher and V. B. Prakapenka, "*DIOPTAS*: A program for reduction of two-dimensional X-ray diffraction data and data exploration," High Pressure Res. **35**(3), 223–230 (2015).
[17]M. Leitner, T. Leitner, A. Schmon, K. Aziz, and G. Pottlacher, "Thermophysical properties of liquid aluminum," Metall. Mater. Trans. A **48**(6), 3036–3045 (2017).
[18]N. D. Milošević and K. D. Maglić, "Thermophysical properties of solid phase zirconium at high temperatures," Int. J. Thermophys. **27**(4), 1140–1159 (2006).
[19]C. R. Noble, A. T. Anderson, N. R. Barton, J. A. Bramwell, A. Capps, M. H. Chang, J. J. Chou, D. M. Dawson, E. R. Diana, T. A. Dunn, D. R. Faux, A. C. Fisher, P. T. Greene, I. Heinz, Y. Kanarska, S. A. Khairallah, B. T. Liu, J. D. Margraf, A. L. Nichols, R. N. Nourgaliev, M. A. Puso, J. F. Reus, P. B. Robinson, A. I. Shestakov, J. M. Solberg, D. Taller, P. H. Tsuji, C. A. White, and J. L. White, *ALE3D: An Arbitrary Lagrangian-Eulerian Multi-Physics Code* (Lawrence Livermore National Lab. (LLNL), Livermore, CA, 2017).
[20]M. R. Armstrong, H. B. Radousky, R. A. Austin, O. Tschauner, S. Brown, A. E. Gleason, N. Goldman, E. Granados, P. Grivickas, N. Holtgrewe, M. P. Kroonblawd, H. J. Lee, S. Lobanov, B. Nagler, I. Nam, V. Prakapenka, C. Prescher, E. J. Reed, E. Stavrou, P. Walter, A. F. Goncharov, and J. L. Belof, "Highly ordered graphite (HOPG) to hexagonal diamond (lonsdaleite) phase transition observed on picosecond time scales using ultrafast x-ray diffraction," J. Appl. Phys. **132**(5), 055901 (2022).
[21]D. J. Steinberg, S. Cochran, and M. W. Guinan, "A constitutive model for metals applicable at high-strain rate," J. Appl. Phys. **51**(3), 1498–1504 (1980).
[22]D. J. Steinberg, *Equation of State and Strength Properties of Selected Materials* (Lawrence Livermore National Laboratory Livermore, 1996).
[23]C. W. Greeff, "Phase changes and the equation of state of Zr," Modell. Simul. Mater. Sci. Eng. **13**(7), 1015–1027 (2005).
[24]K. Suzuki, Y. Matsuki, K. Masaki, M. Sato, and M. Kuroda, "Tensile and microbend tests of pure aluminum foils with different thicknesses," Mater. Sci. Eng. A **513–514**, 77–82 (2009).
[25]P. T. Summers, Y. Chen, C. M. Rippe, B. Allen, A. P. Mouritz, S. W. Case, and B. Y. Lattimer, "Overview of aluminum alloy mechanical properties during and after fires," Fire Sci. Rev. **4**(1), 3 (2015).
[26]P. G. Heighway, M. Sliwa, D. McGonegle, C. Wehrenberg, C. A. Bolme, J. Eggert, A. Higginbotham, A. Lazicki, H. J. Lee, B. Nagler, H.-S. Park, R. E. Rudd, R. F. Smith, M. J. Suggit, D. Swift, F. Tavella, B. A. Remington, and J. S. Wark, "Nonisentropic release of a shocked solid," Phys. Rev. Lett. **123**(24), 245501 (2019).
[27]A. Strachan, T. Çağın, and W. A. Goddard, "Critical behavior in spallation failure of metals," Phys. Rev. B **63**(6), 060103 (2001).
[28]N. A. Inogamov, V. V. Zhakhovskii, and V. A. Khokhlov, "Jet formation in spallation of metal film from substrate under action of femtosecond laser pulse," J. Exp. Theor. Phys. **120**(1), 15–48 (2015).
[29]H. Hwang, E. Galtier, H. Cynn, I. Eom, S. H. Chun, Y. Bang, G. C. Hwang, J. Choi, T. Kim, M. Kong, S. Kwon, K. Kang, H. J. Lee, C. Park, J. I. Lee, Y. Lee, W. Yang, S.-H. Shim, T. Vogt, S. Kim, J. Park, S. Kim, D. Nam, J. H. Lee, H. Hyun, M. Kim, T.-Y. Koo, C.-C. Kao, T. Sekine, and Y. Lee, "Subnanosecond phase transition dynamics in laser-shocked iron," Sci. Adv. **6**(23), eaaz5132 (2020).
[30]D. Kim, S. J. Tracy, R. F. Smith, A. E. Gleason, C. A. Bolme, V. B. Prakapenka, K. Appel, S. Speziale, J. K. Wicks, E. J. Berryman, S. K. Han, M. O. Schoelmerich, H. J. Lee, B. Nagler, E. F. Cunningham, M. C. Akin, P. D. Asimow, J. H. Eggert, and T. S. Duffy, "Femtosecond X-ray diffraction of laser-shocked forsterite (Mg_2SiO_4) to 122 GPa," J. Geophys. Res. Solid Earth **126**(1), e2020JB020337, https://doi.org/10.1029/2020JB020337 (2021).
[31]K. Katagiri, N. Ozaki, S. Ohmura, B. Albertazzi, Y. Hironaka, Y. Inubushi, K. Ishida, M. Koenig, K. Miyanishi, H. Nakamura, M. Nishikino, T. Okuchi, T. Sato, Y. Seto, K. Shigemori, K. Sueda, Y. Tange, T. Togashi, Y. Umeda, M. Yabashi, T. Yabuuchi, and R. Kodama, "Liquid structure of tantalum under internal negative pressure," Phys. Rev. Lett. **126**(17), 175503 (2021).
[32]G. S. Collins, H. J. Melosh, and G. R. Osinski, "The impact-cratering process," Elements **8**(1), 25–30 (2012).
[33]G. R. Osinski, R. A. F. Grieve, G. S. Collins, C. Marion, and P. Sylvester, "The effect of target lithology on the products of impact melting," Meteorit. Planet. Sci. **43**(12), 1939–1954 (2008).
[34]S. M. Tikoo, B. P. Weiss, D. L. Shuster, C. Suavet, H. Wang, and T. L. Grove, "A two-billion-year history for the lunar dynamo," Sci. Adv. **9**(3), e1700207 (2017).
[35]J. Gattacceca, M. Boustie, L. Hood, J.-P. Cuq-Lelandais, M. Fuller, N. S. Bezaeva, T. de Resseguier, and L. Berthe, "Can the lunar crust be magnetized by shock: Experimental groundtruth," Earth Planet. Sci. Lett. **299**(1–2), 42–53 (2010).

08 August 2025 08:15:29

© Author(s) 2024